An EBSD-calibrated subgrain-size piezometer

R.M. Goddard[1], L. Hansen[1,2], D. Wallis[3,4], M. Stipp[5], C.W. Holyoke, III[6], K.M. Kumamoto[1], & D.L. Kohlstedt[2]

[1]University of Oxford, Department of Earth Sciences, South Parks Road, Oxford, OX1 3AN, UK
[2]University of Minnesota, Department of Earth and Environmental Sciences, University of Minnesota – Twin Cities, Minneapolis, Minnesota, USA
[3]Department of Earth Sciences, Utrecht University, Utrecht, 3584 CB, The Netherlands.
[4]University of Cambridge, Department of Earth Sciences, University of Cambridge, Cambridge, CB2 3EQ, U.K
[5]University of Halle, Department of Geosciences and Geography, Von-Seckendorff-Platz 3, 06120 Halle (Saale), Germany
[6]University of Akron, Department of Geosciences, 302 Buchtel Common, Akron, OH 44325-4101 USA

Contents of this file

Introduction

Supplementary material provides descriptions of how to execute the MATLAB® scripts (Text S1); discussion of the choice of shear moduli and Burgers vectors (Text S2); a methodology for high-angular resolution EBSD (HR-EBSD) used to test the angular resolution of the data (Text S3, Figure S6); mechanical data for the experiment in Qz-2, which is published for the first time in this study (Figure S1); analysis on the effect of EBSD step-size on measurements of subgrain size (Figure S2); analysis on the effect of map area on the measurements of subgrain size (Figure S3); examples of samples re-mapped as the area-analysis suggest the maps were too small to capture a representative subgrain-size (Figure S4); analysis on the size of the critical misorientation angle used to define a subgrain boundary (Figure S5): and table of experimental conditions for each of the samples (Table S1).

Text S1: Instructions for using MATLAB® scripts

Codes will be assessable on GitHub, following the link:

https://github.com/RellieGoddard/SGPiezometry.git

The MATLAB® codes provided can be used on polymineralic samples. However, large poorly indexed areas will affect the line intercept length. We recommend that you update and run the scripts in the following order:

1) Ensure MTEX (Version 5.1.1) is running and the following scripts are within the folder: *ProcessEBSD_fun.m, LinearIntercepts_fun.m, No_intercepts_check.m, undersampling.fun.m, Undersampling_Step_Size.m, Area_Analysis_reduction.m, ProcessEBSD_LinearIntercepts.m, Stress_Calulation_fun.m.*

2) The *ProcessEBSD_fun.m* script imports the EBSD data. It cleans the data by removing single pixels known as 'wildspikes' as well as grains, which are less than three pixels in size described as 'shards'**.** No modifications are required for this script but, if desired, there is the ability to expand into no-indexed regions by modifying the 'threshold' section. The higher the threshold value the more of the non-index areas are infilled. A successfully run script should include the following outputs: structures containing information on EBSD, grains, and subgrains, a phase map if input **Phase_map** = [1], and a band contrast map if input **Band_contrast** = [1].

3) Run *No_intercepts_check.m*. This function checks the number of intercepts required to accurately capture the subgrain size. Required user inputs: **nx_max, gb_min, sg_min, cutoff, phase**, **crystal**, **test, include_low**, **CS, pname, fname.**

   a) **nx_max:** The maximum number of intercepts that you want to test (recommended to start at either 30 or 40)

   b) **gb_min:** Minimum misorientation angle to define a grain boundary in degrees (used for constructing maps).

   c) **sg_min:** Minimum misorientation angle to define a subgrain boundary in degrees (only used for constructing maps).

d) **cutoff:** minimum misorientation angle to define a subgrain boundary in degrees. Used for piezometer calculations, recommended value is 1.

e) **phase:** name of phase of interest.

f) **crystal:** crystal system of the phase of interest.

g) **test:** when set to 1, reduces the size of the input EBSD map by taking every tenth pixel in both the horizontal and vertical direction. Can be utilized to ensure the script runs correctly for a new sample file or for troubleshooting. During full analysis, test should be set to 0.

h) **include_low:** the choice of if you want to test very low numbers of intercepts (1–9). To include set to 1. Otherwise, set to 0.

i) **CS:** crystal symmetry class for all indexed phases in EBSD amps.

j) **pname:** path to data**.**

k) **Fname:** file name combined with path.

Expected results: figures showing the line intercepts on top of EBSD data for each iteration, a figure showing the mean line intercept length against the no. of intercepts, and a figure showing the change in mean line intercept length relative to last.

The test is successful if the measured mean line-intercept length stabilises (± 2.5 relative to previous value). If the mean line-intercept does not stabilise, increase **nx_max** and run again.

4) Run *Undersampling_Step_Size.m*. This script tests that the step-size is small enough, that is, the spatial resolution is high enough, to capture the subgrains. Required user inputs: **nx, Int_max, Image_title, Header_size, gb_min, sg_min, cutoff, phase, crystal, test, Phase_map, Band_contrast, CS, pname, fname.**

a) **nx:** The number of intercept lines, chosen based on analysis from *No_intercepts_check.m*.

b) **Int_max:** the number of times you want to reduce the step-size. The step-size at an iteration will be **Int_max** multiplied by the original step-size.

c) **Image_title:** Title for figure

d) **Header_size:** Number of lines, up to and including the line starting with '*phase*' in the *.ctf* file (open in Notepad)

Expected results: a figure showing the intercept variation factor plotted against the number of pixels per intercept. If **Phase_map** = 1 and **Band_contrast** = 1 these maps will be additional outputs.

The test is successful if the measured mean intercept length is not sensitive to the effective step size, which is represented by the presence of an asymptote at an intercept variation factor of 1. If such an asymptote doesn't exist then either re-map the sample, using a smaller step size, or use the subgrain-size stress measurement as a lower bound.

5) Run *Area_Analysis_reduction.m.* This script tests whether the map is large enough to capture the true subgrain size. Required user inputs: **nx, gb_min, sg_min, cutoff, phase, crystal, test, Phase_map, Band_contrast, CS, pname, fname.**

Expected results: an EBSD map for each analysis is outputted with a red box outlining the analysed subarea and a figure showing the intercept analysis of the final subarea. A figure showing the mean line intercept length plotted against the area as a percentage of the original map. On the right axis of the same figure the % change of the mean line intercepts length relative to the full map is plotted against map area.

The test is successful if, as the size of the sub-area increases, the mean intercept length asymptotically approaches the mean for the entire map. For all the samples included in the subgrain-size piezometer, the % change in mean line intercept length relative to the full map was ≤ 5% for a 20% reduction in map area. If the mean line intercept length changes significantly when the map size is reduced then more maps or larger maps are required to accurately capture the subgrain size.

6) Run *ProcessEBSD_LinearIntercepts.m*. This script measures the mean line intercepts between different subgrain boundaries. Required user inputs: **nx, gb_min, sg_min, cutoff, phase, crystal, test, Phase_map, Band_contrast, Check_different_misorientation, SG_piezometer, Piezometer_choice**

    a) **Check_different_misorientation:** To measure the mean line intercept length for minimum misorientation angle between 1 and 10 degrees, set to 1. Otherwise, set to 0.

    b) **SG_piezometer**: To calculate equivalent stress straight from measured subgrain size, set to 1. Otherwise set to 0.

    c) **Peizometer_choice**: If SG_piezometer = 1, **Piezometer_choice** sets which piezometer to use when calculating stress. If using Equation 1, which includes the Holyoke and Kronenberg (2010) friction correction, then **Piezometer_choice** = 1. If using Equation 2, which doesn't have the Holyoke and Kronenberg (2010) friction correction, then **Piezometer_choice** = 2.

    d) **Burgers**: Burgers vector of phase of interest

    e) **Shear_M**: shear modulus of the phase of interest

Expected results: Firstly, if input **Check_different_misorientation** = [1], a plot of mean line intercept length (y-axis) plotted against the defined critical misorientation angle (x-axis). A sample which contains subrgains will show smaller mean line intercept lengths for critical misorientation angles of < 5° than at 10°. Secondly, a figure of the intercept analysis and a histogram of the line intercept lengths including the calculated arithmetic mean. Finally, optional outputs included a band contrast map and a phase map if inputs **Band_contrast** and **Phase_map** both = [1]. If **SG_piezometer** = 1, a stress calculated from one of the Goddard et al., 2020 subgrain-size piezometer will also be outputted.

Text S2: Shear moduli and Burger's vector values

The Burger vector used for quartz was 5.10×10^{-4} µm (Deer et al., 1992, pp 458), which is an average of the *a* (4.9×10^{-4} µm) and *c* (5.4×10^{-4} µm) unit cell dimensions. For olivine, a Burgers vector of 5×10^{-4} µm (Deer et al., 1992, pp 447) was used, which corresponds to the *a* unit cell dimension. These Burgers vectors were chosen as they represent the dominant dislocations active within the conditions of the subgrain-size piezometer. The shear modulus for quartz, 4.2×10^4 MPa, was calculated from wave velocities at a confining pressure of 400 MPa (Birch, Table 7–16 in Clark, 1966). For olivine, shear moduli of 7.78×10^4 and 6.26×10^4 MPa were taken for Fo_{90} and the Fo_{50}, respectively (Mao et al., 2015), corresponding to room temperature and pressure. Although the shear modulus for olivine does have a pressure dependence the change within our pressure range (at room temperature) is <4 % (Abramson et al., 1997); therefore, the shear moduli for olivine remain those at room pressure.

To test the effect of temperature on the subgrain-size piezometric equation, we calculated the shear moduli for Fo_{90} and Fo_{50} at 1250°C as 6.53×10^4 and 5.01×10^4 MPa, respectively (Mao et al., 2015). The shear modulus of quartz remains that at room temperature as it is almost temperature-independent (Peng & Redfern, 2013). The temperature-modified subgrain-size piezometers are $\frac{\lambda}{b} = 10^{0.8 \pm 0.8} \left(\frac{\sigma}{\mu}\right)^{-1.2 \pm 0.3}$ when using Holyoke and Kronenberg (2010) correction and $\frac{\lambda}{b} = 10^{1.1 \pm 0.9} \left(\frac{\sigma}{\mu}\right)^{-1.1 \pm 0.4}$ without this correction. These new equations are within error of the room-temperature subgrain-size piezometer. Hence, the shear moduli used in our work remain those of a mineral at room temperature .

Text S3: Method, High-angular resolution EBSD

We reanalysed a number of samples with high-angular resolution EBSD (HR-EBSD) to assess the impact of orientation noise on the measured subgrain sizes. Recently, HR-EBSD based on the approach of Wilkinson et al. (2006) and Britton and Wilkinson (2011, 2012) has been adapted for geological materials including olivine (Wallis et al., 2016) and quartz (Wallis et al., 2017). The high-

angular precision is beneficial for subgrain-size analysis because it removes noise that otherwise may have been wrongly identified as subgrain boundaries in traditional EBSD. HR-EBSD uses cross-correlation between similar features in adjacent electron backscatter diffraction patterns to improve the angular resolution of standard EBSD (Britton & Wilkinson, 2012; Wallis et al., 2016; Wilkinson, 1996; Wilkinson & Randman, 2010). During conventional Hough-based EBSD, measurements of the misorientation angle between two pixels is limited to a precision of 0.2–0.5° by the process of determining the band positions in Hough-space (Humphreys, 2004; Wilkinson & Randman, 2010). In HR-EBSD, the Hough transform is only used to determine the orientation of a single reference point within each grain (Britton & Wilkinson, 2011; Wilkinson et al., 2006). The orientations of all other pixels in the grain are then found by cross-correlating regions of interest (ROIs) within each EBSP with the same regions in the reference EBSP. A displacement gradient tensor is fitted to the shifts in the positions of the ROIs in each pattern, from which the lattice rotations relative to the reference point can be calculated (Britton & Wilkinson, 2011, 2012; Wilkinson et al., 2006). While this method improves the precision of misorientation angles to the order of 0.01° (Britton & Wilkinson, 2012; Wallis et al., 2016; Wilkinson, 1996; Wilkinson & Randman, 2010), it significantly increases the processing time.

We re-processed the data from two samples using HR-EBSD to test whether conventional EBSD measurements are sufficient for subgrain analysis. Figure S6 presents a comparison of subgrain sizes measured by EBSD and HR-EBSD in samples TMQ-7 and W-1126. Subgrain sizes measured by HR-EBSD and standard EBSD differ slightly, with a greater divergence as the critical misorientation angle is reduced. For samples TMQ-7 and W-1126 there is a 17% change and a 14% change, respectively, between the subgrain sizes measured by HR-EBSD and standard EBSD when using a critical misorientation angle of 1°. Therefore, the orientation noise in standard EBSD data (which can vary among datasets depending on pattern quality and other acquisition parameters) introduces uncertainty of about 15% in the stress. We conclude that, while HR-EBSD is preferable, conventional EBSD has sufficient angular resolution for our subgrain-size piezometer.
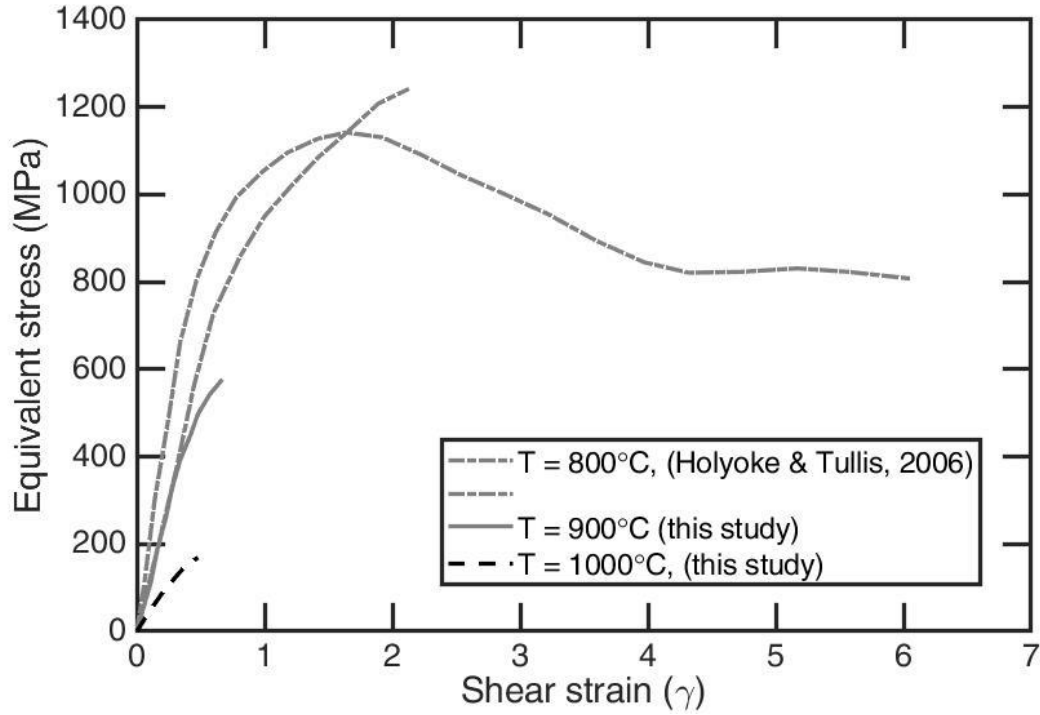
Figure S1 Mechanical data for general shear experiments in Qz-2 some of which are published for the first time in this study. Peak equivalent stress of Black Hills Quartzite sample deformed at a confining pressure of 1500 MPa and an equivalent strain rate of ~ 1.15×10^{-5} s^{-1} and temperatures of between 800°C and 1000°C. The sample in black (W-1134) was included in the calibration of the subgrain-size piezometer. Mechanical data are corrected according to the methods in Holyoke and Kronenberg (2010). Equivalent stress and strain were calculated using the programs RigC and RigS2 by Renee Heilbronner (Heilbronner & Tullis, 2002, 2006).
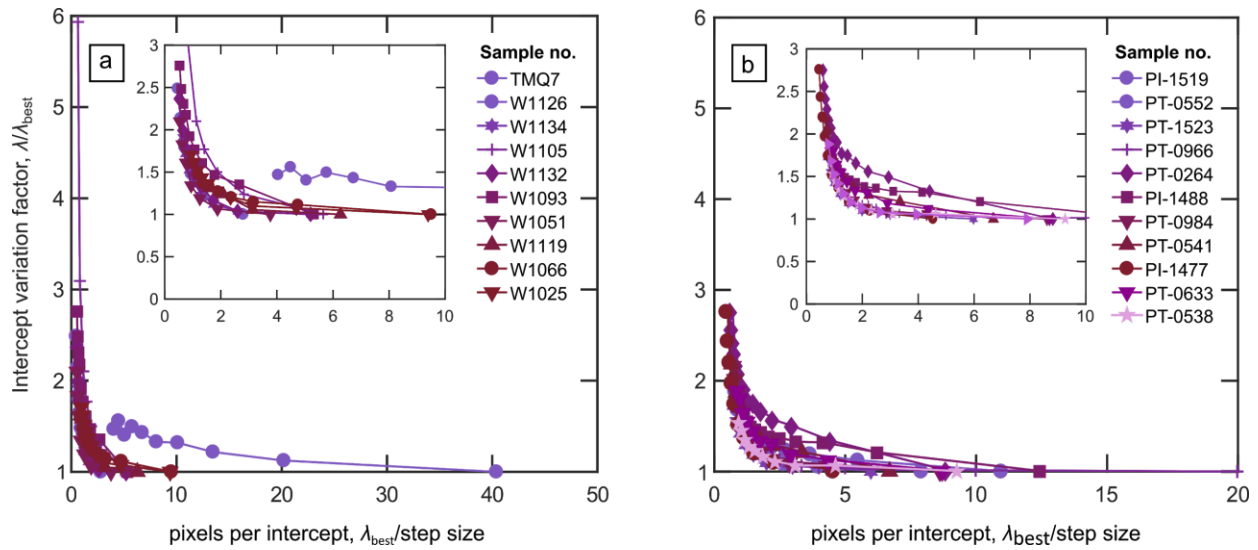
Figure S2: Step-size analysis for (a) quartz samples and (b) olivine samples. The intercept variation factor (λ/λ_{best}), plotted on the vertical axis, represents the degree of change in the mean line-intercept length with change in step size. On the horizontal axis, the pixels per intercept ($\lambda_{best}/(\text{step size})$) is based on the best estimate of mean line-intercept length, that is, the mean intercept length for the smallest step size. For a map with high spatial resolution, the intercept variation factor will stabilise as the pixels per intercept increases.
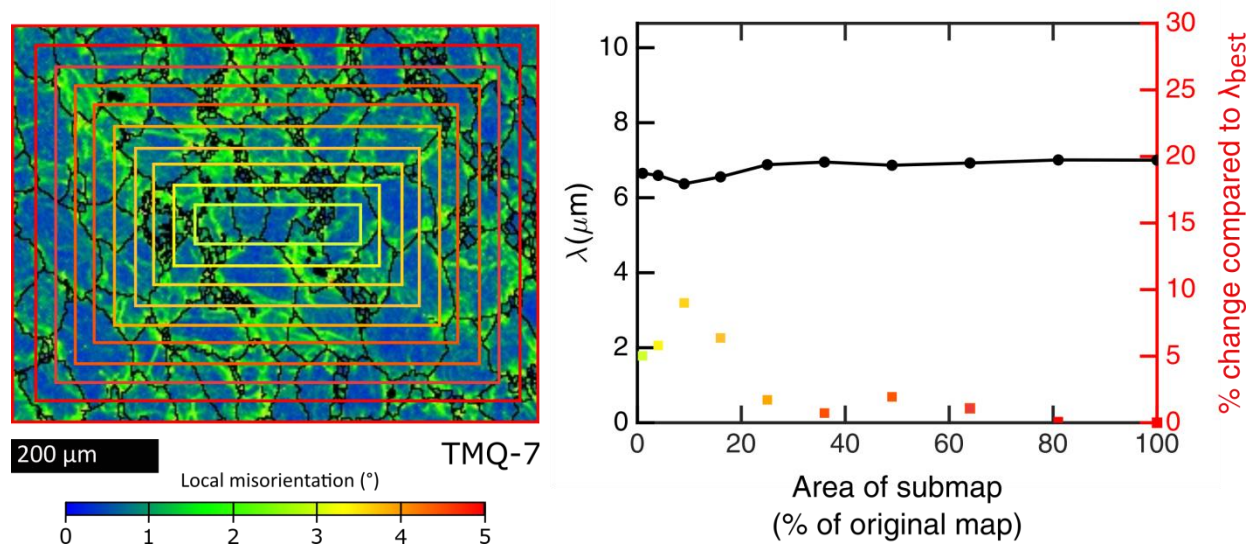
Figure S3: Area analysis of quartz sample TMQ-7 using a critical misorientation angle of 1°. In this analysis, the size of the map is systematically reduced and the mean line-intercept length re-measured. (a) Local misorientation map for TMQ-7. Coloured boxes match the points in Figure S3b and represent the areas mapped at each step. (b) The mean line-intercept length is plotted as black solid circles against the size of the map as a fraction of the size of the original map. The percentage change with respect to the best estimate for subgrain-size (mean line-intercept length of the full map) is plotted against the size of the submap, as solid square points coloured to match the submap areas shown in (a).

Local misorientation (°)

W-1126

σ_1

B

50 μm   Step size = 0.5 μm

C

100 μm   Step size = 1 μm

D

100 μm   Step size = 1 μm

F

100 μm   Step size = 1 μm
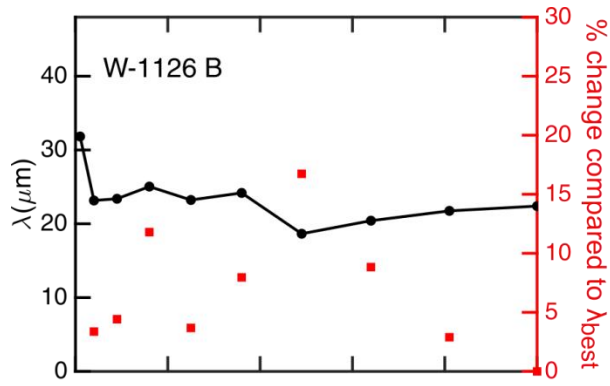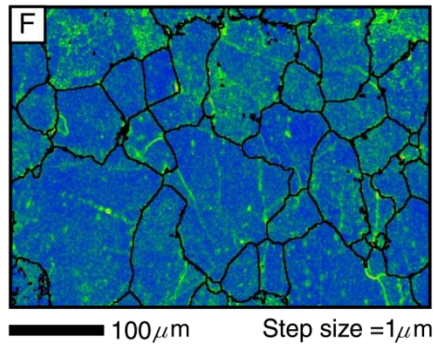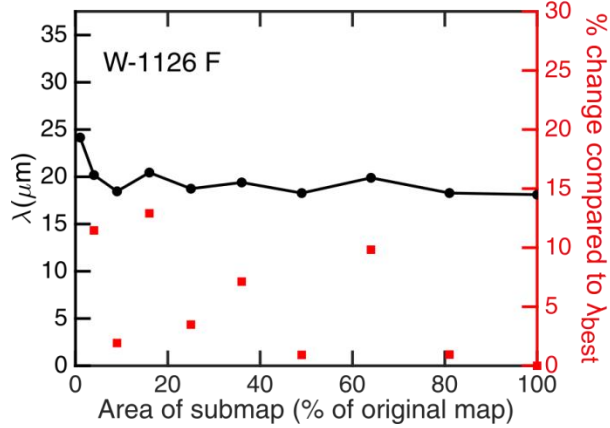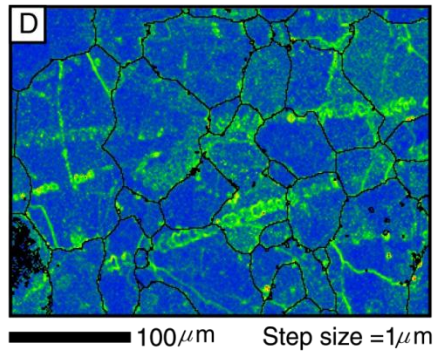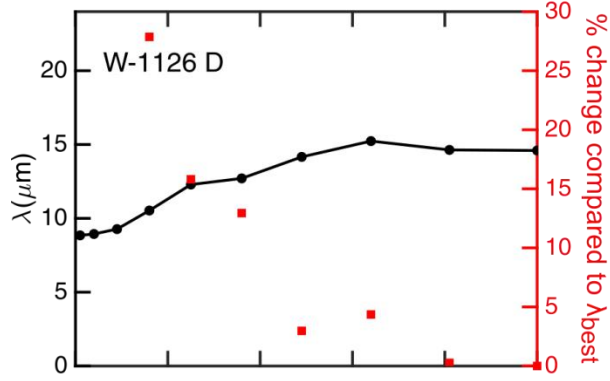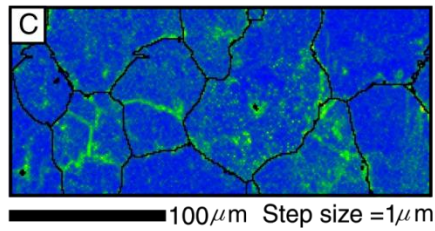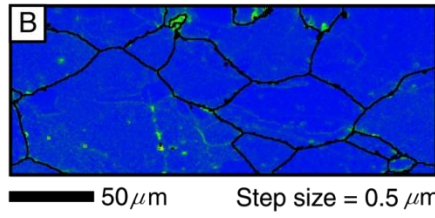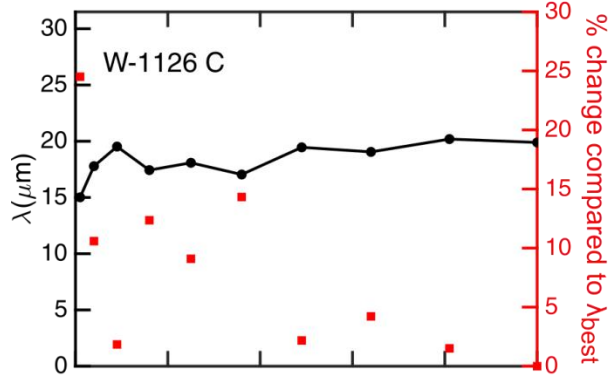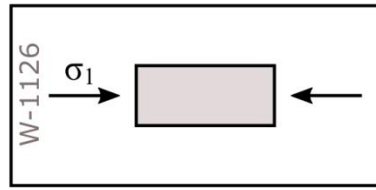
Figure S4: Area analysis of quartz for multiple maps from sample W-1126 (mechanical data W-1116) using a critical misorientation angle of 1°. This analysis is carried out with the same method described in Figure S3. On the right, mean line-intercept length is plotted as black solid circles against the size of the map as a fraction of the size of the original map. The percentage change with respect to the best estimate for subgrain-size (mean line-intercept length of the full map) is plotted along the left-hand axis. Once the percentage change exceeds 30%, it is no longer plotted. Local misorientation maps for each area are shown to the right.
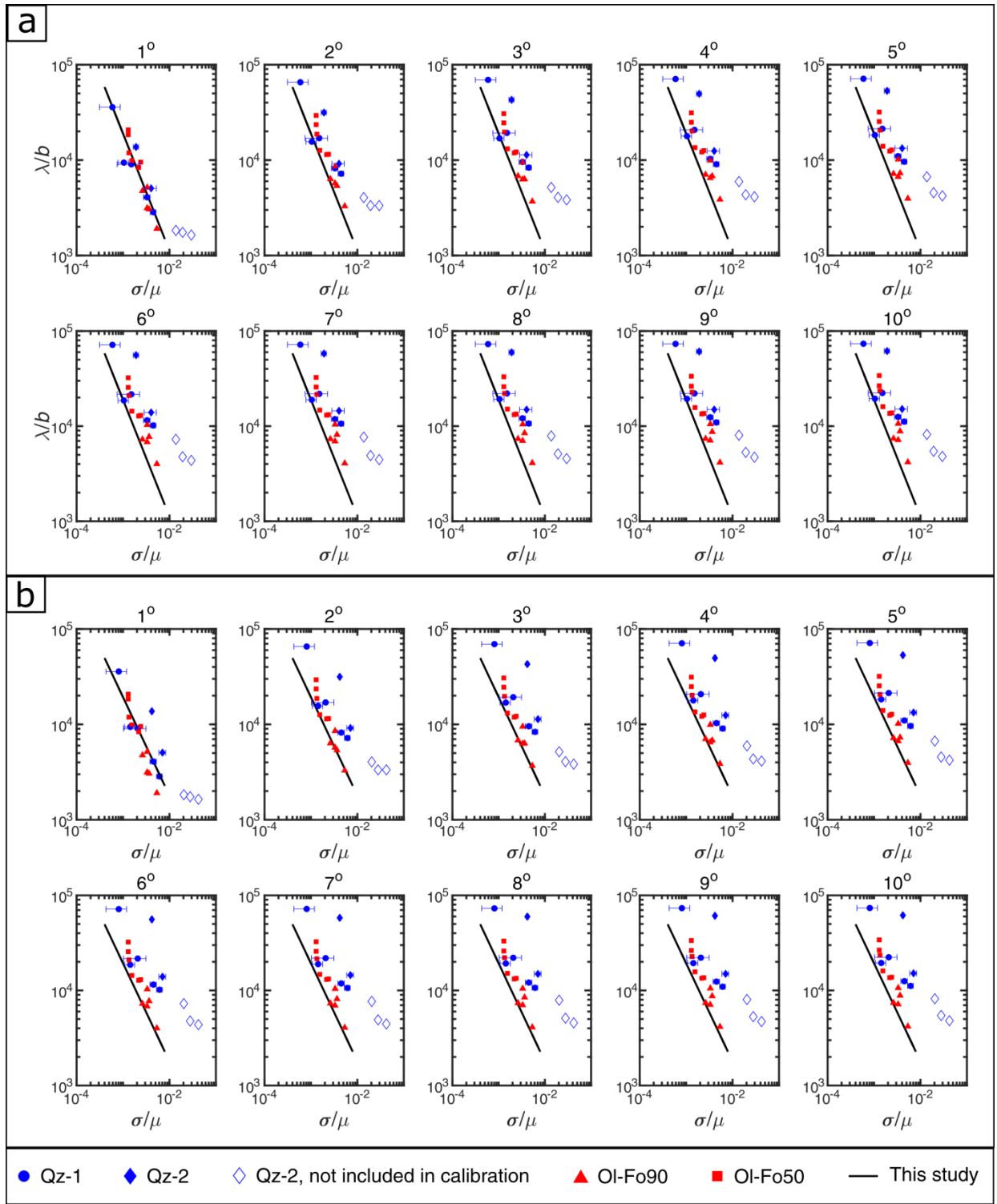
Figure S5: Relationship between mean line intercept length and stress for subgrains with critical misorientations of 1–10° for (a) with the Holyoke and Kronenberg (2010) correction applied to the quartz

data and (b) without the correction. Axes are the same as in Figure 3, as are the Burgers vector and the shear moduli used for each phase. For each map, the critical misorientation angle used to define a subgrain is labelled above the graph. The 1° subgrain-size piezometer is plotted on each graph for comparison.
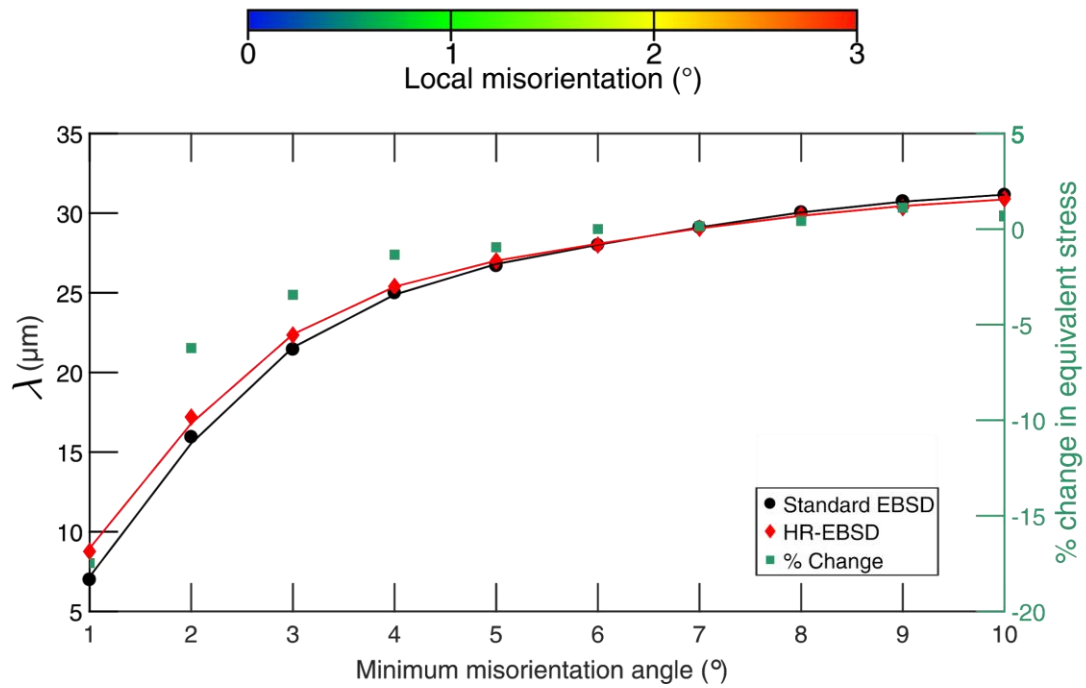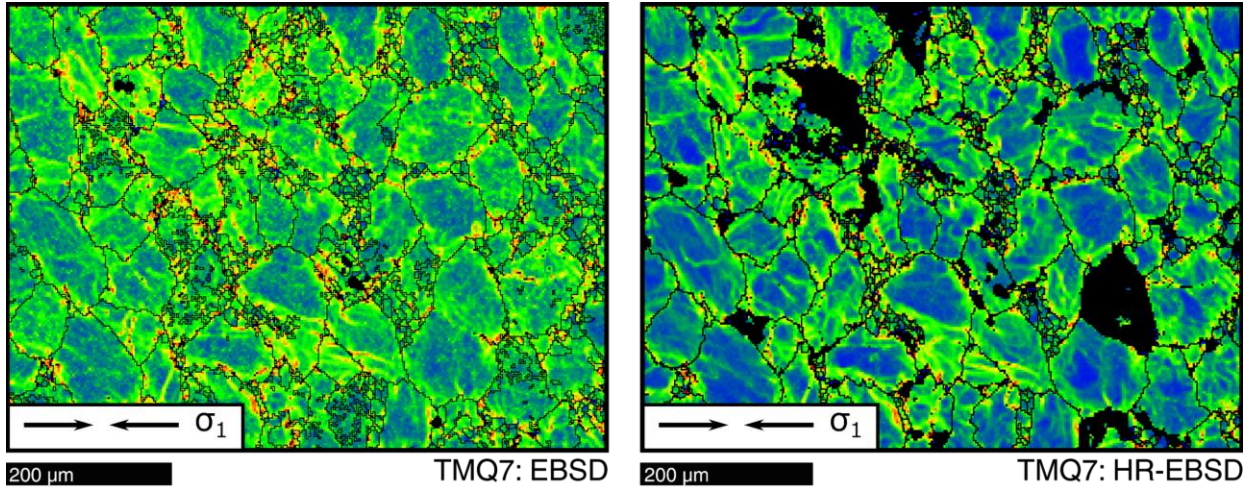
Figure S6: HR-EBSD comparison for quartz sample TMQ-7. Top, are the local misorientation maps are presented for standard EBSD (left) and HR-EBSD (right). Below, the mean line-intercept lengths are compared for a range of minimum misorientation angles for both EBSD and HR-EBSD. The right vertical axis and the green squares track the percent change in equivalent stress as a result of HR-EBSD compared to standard EBSD.

Sample	Mineral	Experiment	Type: Molten Salt Assembly (MSA) or Solid Salt Assembly (SSA)	Temperature [°C]	Confining pressure [MPa]	Equivalent strain rate [10^{-5} s^{-1}]	Total shear strain [1]	Total axial strain [%]	Equivalent flow stress not corrected as per Holyoke and Kronenberg (2010) [MPa]	Equivalent flow stress corrected as per Holyoke and Kronenberg (2010).[MPa]	1° mean line intercept length [λ, μm]	Reference
Dataset 1 (Qz-1)												
W-1116 (W-1126)[2]	Qz	Axial compression	Griggs, MSA	1100	1500	0.021–0.023	-	21 (17)	34 ± 16[3]	25± 12	18.28[4]	Stipp & Tullis (2003)
W-1096 (W-1066)[2]	Qz	Axial compression	Griggs MSA	1100	1500	0.20–0.25	-	32 (31)	60 ± 15[3]	44± 11	4.8	Stipp & Tullis (2003)
W-1025	Qz	Axial compression	Griggs, MSA	1050	1500	0.18–0.24	-	32	87 ± 17	64± 12	4.61[4]	Stipp & Tullis (2003)
W-1051	Qz	Axial compression	Griggs, MSA	1000	1500	1.9–2.9	-	41	189 ± 30[3]	138± 22	2.08[4]	Stipp & Tullis (2003)
W-1119	Qz	Axial compression	Griggs, MSA	1100	1500	18–25	-	36	257 ± 35[3]	188 ± 26	1.45	Stipp & Tullis (2003)
Dataset 2 (Qz-2)												

Sample	Mineral	Experiment	Type	Temperature [°C]	Confining pressure [MPa]	Equivalent strain rate $[10^{-5}$ s$^{-1}]$	Total Shear strain[1]	Total axial strain [%]	Equivalent flow stress [MPa]		1° mean line intercept length (aka. subgrain size) [d_s, μm]	Reference
TMQ-7	Qz	Axial compression	Griggs, SSA	800	1560	0.16	-	15.6	175	80 ± 30	7	Holyoke & Kronenberg (2013)
W-1134	Qz	general, shear	Griggs, SSA	1000	1500	0.16	0.5	-	297	169	2.58	This study, Figure S1
W-1132	Qz	general, shear	Griggs, SSA	900	1500	1.15	0.7	-	856	577	0.93	This study, Figure S1
W-1105	Qz	general, shear	Griggs, SSA	800	1500	1.15	6.1	-	1171	807	0.89	Holyoke & Tullis (2006)
W-1093	Qz	general, shear	Griggs, SSA	800	1500	1.15	2.1	-	1767	1242	0.84	Holyoke & Tullis (2006)
Dataset 3 (Ol)												
Sample	Mineral	Experiment	Type	Temperature [°C]	Confining pressure [MPa]	Equivalent strain rate $[10^{-5}$ s$^{-1}]$	Total Shear strain[1]	Total axial strain [%]	Equivalent flow stress [MPa]		1° mean line intercept length (aka. subgrain size) [d_s, μm]	Reference
PI-1519	Fo$_{90}$	Axial compression	Paterson	1250 ± 2	300 ± 1	9.719	-	<20	204[5] ± 1		2.26	Hansen et al. (2011)
PI-1523	Fo$_{90}$	Axial compression	Paterson	1250 ± 2	300 ± 1	8.912	-	<20	257[5] ± 1		1.49	Hansen et al. (2011)

PI-1488	Fo_{90}	Axial compression	Paterson	1150 ± 2	300 ± 1	0.905	-	5	$258[5] \pm 1$	2.46	Hansen et al. (2011)
PI-1477	Fo_{90}	Axial compression	Paterson	1250 ± 2	300 ± 1	14.40	-	<20	$283[5] \pm 1$	1.45	Hansen et al. (2011)
PT-0966	Fo_{50}	Torsion	Paterson	1200 ± 2	300	147.8	$5.0[6]$	-	81	9.85	Tasaka et al. (2016)
PT-0633	Fo_{50}	Torsion	Paterson	1200 ± 2	250–300	3.6	$8.7[8]$	-	$81[7]$	8.77	Hansen et al. (2012)
PT-0541	Fo_{50}	Torsion	Paterson	1200 ± 2	250–300	4.5	$7.6[8]$	-	$84[7]$	5.66	Hansen et al. (2012)
PT-0538	Fo_{50}	Torsion	Paterson	1200 ± 2	250–300	11.9	$6.8[8]$	-	$97[7]$	4.69	Hansen et al. (2012)
PT-0552	Fo_{50}	Torsion	Paterson	1200 ± 2	250–300	51.1	$8.8[8]$	-	$136[7]$	3.98	Hansen et al. (2012)
PT-984	Fo_{50}	Torsion	Paterson	1200	300	47.7	$4.2[8]$	-	150	4.52	Tasaka et al. (2017)
PT-0264	Fo_{90}	Torsion	Paterson	1200	300	20.2	$3.5[8]$	-	416	0.91	Pommier et al. (2015)

[1] Rounded to 1 d.p.

[2] For Qz-1, the method of correcting for friction alters the microstructures. Therefore, a pair of experiments were conducted at each set of conditions, with one experiment providing the friction correction and the other providing the sample for microstructural analysis (Stipp & Tullis 2003). The first sample name is the sample associated with the mechanical data. The second sample name, in brackets, refers to the sample from which the microstructural analysis has come.

[3] Flow stresses were taken as the average over the interval between 10% and the final strain. The error estimates are based on the maximum stress variations in the study range and on the different frictional correction methods used (see Stipp & Tullis, 2003, for a description of the friction correction methods).

[4] Mean of the sum of all line intercepts from four different maps.

[5] Stress is determined from load measurements using the instantaneous cross-sectional area of the sample. The cross-sectional area is calculated on the assumption of constant volume deformation. Corrections were also made to the measured load for the load supported by the iron jacket and nickel capsules. The stress presented is the last stress felt by the sample.

[6] Shear strain from the crease of the jacket of the sample

[7] Steady state stress, mean of the values measured at the controlling strain rate, see Hansen et al. (2012)

[8] Outer radius shear strain

Table S1: Experimental conditions